the reaction of OH with H_2.[19] The value of T^* for the latter reaction was also below the experimental temperature range. For the reaction of H with CH_4 we found a much higher barrier, 55 kJ mol^{-1}, but for Cl with CH_4, a somewhat lower barrier, 12 kJ mol^{-1}, with little tunneling.[19]

Acknowledgment. We thank the National Sciences and Engineering Research Council of Canada for financial support and H. Furue and A. Mehta for assistance with computations.

Registry No. OH, 3352-57-6; CH_4, 74-82-8.

Kinetics of the Reaction between OH and HO_2 on the Triplet Potential Energy Surface

Carlos Gonzalez,† John Theisen, H. Bernhard Schlegel, William L. Hase,*

Department of Chemistry, Wayne State University, Detroit, Michigan 48202

and E. W. Kaiser

Chemistry Department, Research Staff, Ford Motor Company, Dearborn, Michigan 48121-2053
(Received: August 5, 1991)

Ab initio and rate theory calculations are used to study the OH + $HO_2 \rightarrow O_2 + H_2O$ reaction. The structure and energy are determined for the planar HO···HO_2 hydrogen-bonded complex. At the highest level of theory considered here, PMP4/6-31G**, this complex is more stable than the separated reactants by 5.1 and 9.0 kcal/mol on the $^3A''$ and $^3A'$ potential energy surfaces, respectively. The $^3A''$ surface correlates with the ground electronic state products, and the energy and vibrational frequencies for the reaction transition state on this surface are calculated at the HF/6-31G** and MP2/6-31G** levels. In nonplanar configurations an avoided crossing occurs between the $^3A'$ and $^3A'$ surfaces. The nonplanar ^3A transition state which arises from the $^3A''$ transition state is characterized at both the HF and MP2 levels. However, there is considerable uncertainty regarding the position of the $^3A'$–$^3A''$ avoided crossing. As a result, it is not clear whether the triplet reaction transition state originates from the planar $^3A''$ transition state or the $^3A'$–$^3A''$ avoided crossing. The reaction kinetics on the triplet surface is controlled by the long-range attractive potential and not by the reaction transition state. A vibrationally/rotationally adiabatic model, with proper treatment of electronic degeneracies, gives a reaction rate constant as a function of temperature which agrees within a factor of 2 with the most recent experimental results for the 298–1100 K temperature range. Combining this calculated temperature dependence with the average of all recent experimental measurements of the OH + HO_2 reaction rate at ambient temperature yields the rate constant $k_1 = 7.1 \times 10^{-11}(T/300)^{-0.21} \exp(113/RT)$ cm^3 molecule^{-1} s^{-1}. This expression produces substantially larger rate constants at high temperature than those previously estimated and, we believe, represents a new preferred rate constant for use in combustion modeling.

I. Introduction

The reaction

$$OH + HO_2 \rightarrow H_2O + O_2 \qquad (1)$$

is of interest because of its importance in atmospheric and combustion chemistry and because of its close relationship to peroxy–peroxy radical reactions.[1,2] Reliable measurements of the rate constant for this reaction have proven difficult, particularly at elevated temperatures. The standard procedure for determining k_1 is to measure the loss of OH in excess HO_2.[1,2] From early studies of this type there was some indication that k_1 is pressure dependent between 1 and 1000 Torr; increasing from (5–8) × 10^{-11} cm^3 molecule^{-1} s^{-1} at low pressure[3-7] to (1–2) × 10^{-10} cm^3 molecule^{-1} s^{-1} at high pressure.[8-12] In recent work, Keyser[1] measured k_1 as (1.1 ± 0.3) × 10^{-10} cm^3 molecule^{-1} s^{-1} at 299 K and 1 Torr and Schwab et al.[2] found k_1 to equal $8.0^{+3.0}_{-2.0}$ × 10^{-11} cm^3 molecule^{-1} s^{-1} at 298 K and 2 Torr. These low-pressure values for k_1 are not significantly different from the values measured at high pressure. Thus, the current experimental understanding[1,2] is that the rate constant for reaction 1 exhibits little or no pressure dependence for pressures less than 1000 Torr.

A more problematic issue regarding k_1 is its temperature dependence. This is particularly significant since reaction 1 is an important termination reaction in combustion mechanisms with fuel-lean conditions. The earliest determination of the temperature dependence of k_1 was by Sridharan et al.,[3] who found k_1 to equal (1.7 ± 0.5) × 10^{-11} exp[(416 ± 86)/T] cm^3 molecule^{-1} s^{-1} for T = 252–420 K. In a more recent study Keyser[1] found k_1 to equal (4.8 ± 0.8) × 10^{-11} exp[(250 ± 50)/T] cm^3 molecule^{-1} s^{-1} for the 254–382 K temperature range. These two expressions for k_1 differ by a factor of 1.6 at 300 K with their difference increasing as T increases. Also, neither of these expressions extend into the high-temperature regime of combustion studies.

Theoretical studies have been carried out to assist in interpreting the kinetics for reaction 1.[13-18] The most extensive theoretical work has involved ab initio quantum chemical calculations.[13-15] On the OH + HO_2 singlet potential energy surface, the reactants associate to form the hydrogen trioxide intermediate H_2O_3.[14] The potential energies and structures of different internal rotation

† Current address: Department of Chemistry, Carnegie Mellon University, Pittsburgh, PA 15213.

(1) Keyser, L. F. *J. Phys. Chem.* **1988**, *92*, 1193.
(2) Schwab, J. J.; Brune, W. H.; Anderson, J. G. *J. Phys. Chem.* **1989**, *93*, 1030.
(3) Sridharan, U. C.; Qiu, L. X.; Kaufman, F. *J. Phys. Chem.* **1984**, *88*, 1281.
(4) Sridharan, U. C.; Qiu, L. X.; Kaufman, F. *J. Phys. Chem.* **1981**, *85*, 3361.
(5) Temps, F.; Wagner, H. Gg. *Ber. Bunsen-Ges. Phys. Chem.* **1982**, *86*, 119.
(6) Thrush, B. A.; Wilkinson, J. P. T. *Chem. Phys. Lett.* **1981**, *81*, 1.
(7) Keyser, L. F. *J. Phys. Chem.* **1981**, *85*, 3667.
(8) Kurylo, M. J.; Klais, O.; Laufer, A. H. *J. Phys. Chem.* **1981**, *85*, 3674.
(9) De More, W. B. *J. Phys. Chem.* **1982**, *86*, 121.
(10) Hochnadel, C. J.; Sworski, T. J.; Ogren, P. J. *J. Phys. Chem.* **1980**, *84*, 3274.
(11) Lii, R. R.; Gorse, R. A.; Sauer, M. C.; Gorgen, S. *J. Phys. Chem.* **1980**, *84*, 819.
(12) Burrows, J. P.; Cox, R. A.; Derwent, R. G. *J. Photochem.* **1981**, *16*, 147.
(13) Cremer, D. *J. Chem. Phys.* **1978**, *69*, 4456.
(14) Jackels, C. F.; Phillips, D. H. *J. Chem. Phys.* **1986**, *84*, 5013.
(15) Toohey, D. W.; Anderson, J. G. *J. Phys. Chem.* **1989**, *93*, 1049.
(16) Mozurkewich, M. *J. Phys. Chem.* **1986**, *90*, 2216.
(17) Phillips, L. F. *J. Phys. Chem.* **1990**, *94*, 7482.
(18) Gonzalez, C.; Theisen, J.; Zhu, L.; Schlegel, H. B.; Hase, W. L.; Kaiser, E. W. *J. Phys. Chem.* **1991**, *95*, 6784.

0022-3654/92/2096-1767$03.00/0

conformations of H_2O_3 were studied by Cremer[13] using Hartree–Fock theory with basis sets with and without polarization functions. Electron correlation was treated via many-body perturbation theory. An important finding from this study is the large barriers for simultaneous rotation of both OH groups in hydrogen trioxide.

In a SCF-CI study utilizing basis sets of polarized double-ζ quality, Jackels and Phillips[14] investigated both the HOOOH hydrogen trioxide intermediate and the HO···HO_2 hydrogen-bonded species. The trioxide intermediate was found to be nonplanar, in a ^1A electronic state, and to have an electronic energy 26.4 kcal/mol lower than that of the OH and HO_2 reactants. The hydrogen-bonded species was assumed to be planar and was found to have essentially degenerate $^3A'$ and $^1A'$ states with an electronic energy 4.7 kcal/mol below that of the reactants. Geometries for the hydrogen-bonded $^3A''$ and $^1A''$ excited states were not optimized, but a qualitative analysis showed that they are also bound.

In recent work Toohey and Anderson[15] studied the $^3A'$ and $^3A''$ potential energy surfaces using HF and MP2 theory with the 3-21G** and 6-31G** basis sets. Using HF/6-31G** calculations, geometries were optimized for both the $^3A'$ and $^3A''$ planar HO···HO_2 hydrogen-bonded species. The $^3A'$ HO···HO_2 complex was found to have an electronic binding energy of 6.0 kcal/mol and to be 1.9 kcal/mol lower in energy than the $^3A''$ complex. The $^3A''$ state correlates with the $^3O_2$ and H_2O ground-state products, while the $^3A'$ state is correlated with excited triplet channels which are not energetically accessible at thermal energies. Toohey and Anderson[15] found a planar saddlepoint for reaction on the $^3A''$ surface at the HF/3-21G**, HF/6-31G**, and MP2/6-31G** levels of theory. At the MP2/6-31G** level the transition state has an electronic energy 2.6 kcal/mol higher than that of the reactants. However, because of the size and temperature dependence of k_1, they concluded that the MP2 estimate of the saddlepoint energy is too high and crossing this saddlepoint energy is not rate determining.

Several theoretical studies have dealt with the kinetics of reaction 1. In a model RRKM study, which did not explicitly treat the different singlet and triplet potential energy surfaces involved in OH + HO_2 collisions, Mozurkewich[16] considered the pressure and temperature dependence of reaction 1. In this study it was assumed that the negative temperature dependence required either one or both of the following complex mechanisms:

$$OH + HO_2 \rightleftharpoons HO\cdots HO_2 \rightarrow O_2 + H_2O \quad (2)$$

$$OH + HO_2 \rightleftharpoons HOOOH \rightarrow O_2 + H_2O \quad (3)$$

The hydrogen-bonded species was found to be too weakly bound to produce a significant pressure dependence. Reaction 3 had to be included in the overall mechanism to obtain an observable pressure dependence. In a calculation utilizing their ab initio results, Toohey and Anderson[15] found that the saddlepoint structure and vibrational frequencies for reaction 2 gives an A factor for reaction between OH and HO_2 substantially smaller than the experimental value. Phillips[17] has determined a rate constant for reaction 1 using a modified Langevin collision capture model based on the OH + HO_2 long-range potential and assuming reaction occurs on the singlet surface. Though his calculated rate constant agrees with experiment at 300 K, its temperature dependence does not agree with experiment. Keyser's recent experimental determination[1] of the temperature dependence of reaction 1 is $k_1 = (4.8 \pm 0.8) \times 10^{-11} \exp[(250 \pm 50)/T]$ cm^3 molecule^{-1} s^{-1} for T = 254–382 K. In contrast, Phillips' theoretical model gives $k_1 = 7.5 \times 10^{-11} \exp(76/T)$ cm^3 molecule^{-1} s^{-1} for T = 250–400 K.

In very recent work we performed electronic structure and reaction rate theory calculations to study reaction 1 on the singlet potential energy surface.[18] Structures for the HOOOH hydrogen trioxide intermediate and the reaction transition state for $^1O_2$ + H_2O formation were optimized using HF/6-31G** and MP2/6-31G** theory. MP4 theory with the 6-31G** basis was then used to calculate energies for the MP2 optimized structures. The MP4 0 K barrier height for the reaction transition state is 15.2 kcal/mol. Thus, reaction on the singlet surface to form $^1O_2$ and H_2O is predicted to be *unimportant*, except at highly elevated temperature. Vibrationally quenching of the HOOOH intermediate formed by OH + HO_2 association would lead to the loss of OH and an apparent pressure enhancement of the reaction rate. However, because of the rather shallow potential energy minimum found for H_2O_3 (i.e., ~20–30 kcal/mol),[14,18] helium pressures in excess of 5000 Torr are required to yield noticeable stabilization of H_2O_3 at room temperature (higher temperatures would require higher pressures for stabilization). From our calculations it was concluded that for pressures in the range of several atmospheres and less and for temperatures below 2500 K, OH + HO_2 collisions on the singlet surface do *not* lead to appreciable reaction or loss of reactants. Thus, any reaction for these pressure and temperature conditions is predicted to occur on the triplet potential energy surface. In this paper we present electronic structure and reaction rate theory calculations for reaction 1 on the triplet potential energy surface.

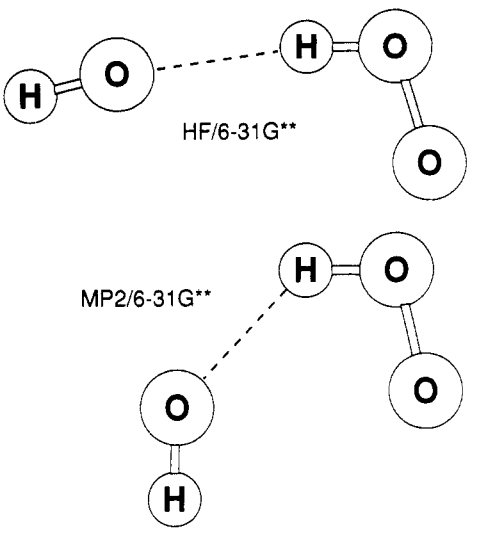

Figure 1. HF and MP2 geometries for the planar $^3A''$ HO···HO_2 complex.

II. Ab Initio Calculations of the Triplet Potential Energy Surfaces

A. Theoretical Method. Ab initio molecular orbital calculations were performed using the GAUSSIAN 88 and 90 system of programs.[19] Fully optimized geometries, harmonic vibrational frequencies, and zero-point energy corrections for the reactants, intermediates, transition structures, and products involved in the reaction between HO_2 and OH (on the triplet surface) were calculated at the Hartree–Fock and MP2 levels using the 6-31G** basis set[20] with analytical derivatives.[21]

Electron correlation was computed with fourth-order Moller–Plesset perturbation theory[22] in the space of single, double, triple, and quadruple excitations using the optimized geometries obtained at the Hartree–Fock and MP2 levels (MP4SDTQ/6-31G**//HF/6-31G** and MP4SDTQ/6-31G**//MP2/6-31G**, respectively). Since the energies were calculated by unrestricted HF and MPn methods, an approximate spin projection method[23] was used to remove contamination from higher spin states (denoted by PMPn in Table I).

B. Planar $^3A''$ Potential Energy Surface. Both HF and MP2 optimized structures for stationary points on the planar $^3A''$ po-

(19) Frisch, M. J.; Head-Gordon, M.; Trucks, G. W.; Foresman, J. B.; Schlegel, H. B.; Raghavachari, K.; Robb, M. A.; Binkley, J. S.; Gonzalez, C.; Defrees, D. J.; Fox, D. J.; Whiteside, R. A.; Seeger, R.; Melius, C. F.; Baker, J.; Martin, R.; Kahn, L. R.; Stewart, J. J. P.; Topiol, S.; Pople, J. A. GAUSSIAN 90; Gaussian, Inc.: Pittsburgh, 1990.

(20) Hariharan, P. C.; Pople, J. A. *Chem. Phys. Lett.* **1972**, *66*, 217.

(21) Schlegel, H. B. *J. Comput. Chem.* **1982**, *3*, 214.

(22) Defrees, D. J.; Raghavachari, K.; Schlegel, H. B.; Pople, J. A. *J. Am. Chem. Soc.* **1982**, *104*, 5576.

(23) Gonzales, C.; Sosa, C.; Schlegel, H. B. *J. Phys. Chem.* **1989**, *93*, 2435 and references therein.

TABLE I: Structures and Energies for the Planar $^3A''$ Potential Energy Surface

coordinate[a]	reactants	complex	trans state	products
R_1	0.971 (0.955)[b]	0.970 (0.954)	0.973 (0.953)	0.960 (0.943)
R_2		2.016 (2.078)	1.332 (1.240)	0.960 (0.943)
R_3	0.975 (0.950)	0.977 (0.951)	1.064 (1.114)	
R_4	1.325 (1.309)	1.322 (1.308)	1.295 (1.259)	1.246 (1.168)
α		138.2 (174.0)	99.1 (101.7)	103.8 (106.0)
β		133.7 (171.8)	160.2 (167.6)	
γ	104.5 (105.9)	103.6 (105.7)	107.7 (109.9)	
theory[c]				
HF	-225.564 97[d]	-225.571 52	-225.533 14	-225.641 53 (-149.617 91)[e]
MP2	-226.047 61	-226.056 32	-226.043 64	-226.176 77 (-149.954 32)
MP3	-226.060 93	-226.068 87	-226.051 77	-226.167 50 (-149.941 41)
MP4	-226.081 18	-226.089 70	-226.077 61	-226.196 02 (-149.964 78)
PHF	-225.570 40	-225.574 30	-225.547 23	-225.640 82 (-149.617 20)
PMP2	-226.044 31	-226.052 04	-226.041 38	-226.178 12 (-149.955 67)
PMP3	-226.063 02	-226.070 49	-226.054 77	-226.169 86 (-149.943 77)
PMP4	-226.083 27	-226.091 31	-226.080 61	-226.198 38 (-149.967 14)

[a] Bond distances are in units of angstroms and angles in degrees. Using the atom numbering $H_1O_2H_3O_4O_5$, the internal coordinates are defined as follows: $R_1 = H_1$–O_2, $R_2 = O_2$–H_3, $R_3 = H_3$–O_4, $R_4 = O_4$–O_5, $\alpha = H_1$–O_2–H_3, $\beta = O_2$–H_3–O_4 and $\gamma = H_3$–O_4–O_5. [b] Both MP2/6-31G** and HF/6-31G** optimized geometries are given. The HF geometries are in parentheses. [c] Energies are given in hartrees (1 hartree = 627.51 kcal/mol). The HF energies are calculated at the HF geometries. The remaining energies are calculated at the MP2 geometries. The MP2 energy is full; the PHF, MP3, MP4, and all PMPn energies are frozen core. [d] The OH and HO_2 individual energies are given in ref 18. [e] The $^3O_2$ energies are given in parentheses. The H_2O energies are given in ref 18.

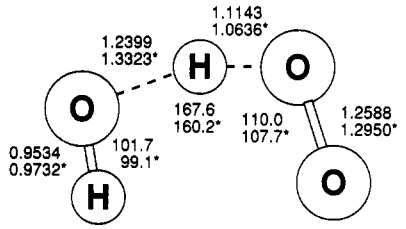

Figure 2. Calculated HF and MP2 (indicated by asterisks) geometries for the planar $^3A''$ reaction transition state.

tential energy surface are listed in Table I. Also included are energies for these stationary points evaluated at different levels of theory. HF and MP2 vibrational frequencies for the planar $^3A''$ stationary points are listed in Table II. Structures for the complex and transition state are illustrated in Figures 1 and 2, respectively. The ab initio structures and frequencies given here for the reactants and for the H_2O product were compared with experiment and other ab initio calculations in our previous work on the singlet OH + HO_2 surface.[18] Also given in this previous work are energies for the reactants and H_2O product. The MP2 bond length and harmonic vibrational frequency for the $^3O_2$ product are in good agreement with the experimental values of 1.2075 Å and 1580 cm^{-1}.[24]

An important finding from the vibrational frequency calculations is that one of the out-of-plane torsional frequencies for both the complex and transition state is imaginary. At the HF level of theory the planar complex is not a true minimum, and both HF and MP2 theory show that the planar transition state is not a true saddlepoint. (MP2 vibrational frequencies were not determined for the planar complex.) Thus, the true reaction path on the $^3A''$ surface is predicted to have a nonplanar configuration.

Before continuing this discussion of the planar $^3A''$ surface, it should be noted that in previous work Toohey and Anderson[15] also studied the complex and transition state at the HF/6-31G** level and the transition state at the MP2/6-31G** level. Our HF and MP2 energies for the complex and transition state are identical to the values they report. The bond lengths they list for the complex and transition state are identical to ours, but for the complex there are differences as large as 0.9° between their α, β, and γ angles and the values we find. This is not unexpected, since the potential energy surface for the complex is very flat. A difference between our work and that of Toohey and Anderson[15] is that they report the planar $^3A''$ HF and MP2 transition states as true saddlepoints. In addition, the HF/6-31G** frequencies they reported for the $^3A''$ transition state are only in qualitative agreement with the ones we list in Table II. Their HF/6-31G** transition-state vibrational frequencies, in the same sequence as ours in Table II, are 3672, 572, 4672*i*, 1242, 1472, 783, 172, no entry, and 582 cm^{-1}. They only list eight frequencies and do not report a value for the out-of-plane mode for which we find an imaginary frequency.

(24) Rosen, B. *Spectroscopic Data Relative to Diatomic Molecules*; Pergamon: New York, 1970.

TABLE II: MP2 and HF Vibrational Frequencies for the Planar $^3A''$ Potential Energy Surface[a]

motion	reactants	complex	trans state	products
	A′ Symmetry Vibrations[b]			
O–H stretch	3847 (4052)	(4068)	(4086)	4033 (4264)[c]
O···H stretch		(157)	(636)	3895 (4147)
O–H stretch of HO_2	3713 (4074)	(4073)	(5185*i*)	
O–O stretch	1238 (1251)	(1259)	(1380)	1413 (1998)
O–O–H bend	1460 (1602)	(1645)	(1636)	
H–O···H bend		(265)	(867)	1684 (1770)
O···H–O bend		(39)	(189)	
	A″ Symmetry Vibrations[b]			
H–O···H bend		(326*i*)	(99*i*)	
O···H–O bend		(324)	(647)	

[a] Frequencies are in cm^{-1}. The MP2/6-31G** and HF/6-31G** (in parentheses) vibrational frequencies were calculated at the MP2 and HF optimized geometries, respectively. [b] The A′ and A″ symmetries refer to the complex and transition-state vibrations.

Both the HF and MP2 results in Table I show that the geometries of OH and HO_2 are only slightly distorted in forming the HO···HO_2 complex. However, the intermolecular geometry (Figure 1) for the complex is different for these two levels of theory. The O···H distance is larger for the HF calculation. Also, the H–O···H–O framework is nearly linear at the HF level but highly bent at the MP2 level of theory. As discussed previously by Toohey and Anderson,[15] HF and MP2 theory give different transition state structures. The MP2 calculation gives a much earlier transition state along the reaction path than does the HF calculation. Though the α, β, and γ angles are similar for the two transition states, a comparison of the R_2, R_3, and R_4 distances in Table I and Figure 2 clearly shows that the MP2 transition state is earlier.

Relative electronic energies between stationary points on the planar $^3A''$ potential energy surface are listed in Table III. The relative energy of the complex is not strongly dependent on the level of theory. In contrast, the transition-state energy is strongly affected by the level of theory. The MP2 barrier height of 2.48 kcal/mol agrees with the MP2 barrier reported by Toohey and Anderson.[15] However, our MP4 (SDTQ) barrier of 2.24 kcal/mol

TABLE III: Relative Electronic Energies for the Planar $^3A''$ Potential Energy Surface[a]

theory	reactants	complex	trans state	products
HF	0	-4.11	19.97	-48.04
MP2	0	-5.47	2.49	-81.05
MP3	0	-4.98	5.75	-66.87
MP4	0	-5.35	2.24	-72.06
PHF	0	-2.45	14.54	-44.20
PMP2	0	-4.85	1.84	-83.97
PMP3	0	-4.69	5.18	-67.04
PMP4	0	-5.05	1.67	-72.23

[a] Zero-point energies are not included. Energies are in kcal/mol.

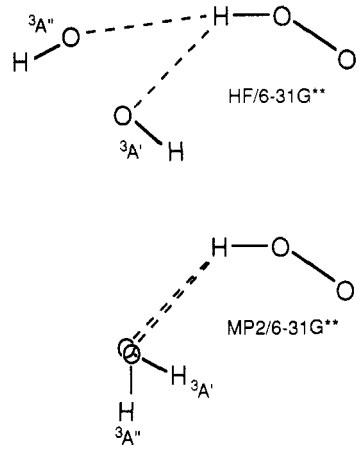

Figure 3. Comparison between HF and MP2 geometries for the $^3A'$ and $^3A''$ hydrogen-bonded complexes.

differs from the 3.8 kcal/mol MP4 (SDQ) barrier they found. Including triples in the MP4 calculation lowers the barrier. For the highest level of theory used here, i.e., PMP4, the planar $^3A''$ transition state has a barrier of 1.67 kcal/mol. The OH + HO_2 → H_2O + $^3O_2$ experimental heat of reaction at 0 K is -69.5 kcal/mol. (The 0 K experimental heats of formation for OH, HO_2, $^3O_2$, and H_2O are 9.25,[25] 3.2,[26] 0.00,[25] and -57.10 kcal/mol,[25] respectively). The MP2 reactant and product vibrational frequencies in Table II and the product relative electronic energies in Table III can be used to calculate values for this heat of reaction. The resulting PMP4 0 K heat of reaction is -71.4 kcal/mol and in very good agreement with experiment.

C. Planar $^3A'$ Hydrogen-Bonded Complex. Both HF and MP2 optimized geometries were determined for the planar $^3A'$ hydrogen-bonded complex, and they are listed in Table IV. For the $^3A''$ complex (Table I), HF and MP2 theory give different values for both the α and β angles. In contrast, for the $^3A'$ complex, there is very little difference between the HF and MP2 values for the α and β angles. The only significant difference between the HF and MP2 geometries of the $^3A'$ complex is in the O···H distance, which is 0.13 Å shorter at the MP2 level. A comparison between the HF and MP2 geometries for the $^3A''$ and $^3A'$ complexes is given in Figure 3. At the HF level the geometries of the two complexes are quite different. However, the MP2 calculations give $^3A''$ and $^3A'$ complexes with rather similar geometries.

Electronic binding energies, evaluated at different levels of theory, are compared in Table IV for the planar $^3A'$ hydrogen-bonded complex. Treating electron correlation by Moller–Plesset theory increases the binding energy. Comparing the binding energies in Tables III and IV for the $^3A''$ and $^3A'$ complexes shows that the $^3A'$ complex is more strongly bound. However, the actual difference between the two binding energies depends on the level of theory. For the highest level of theory used here, PMP4, there is a 3.9 kcal/mol difference between the binding energies for the $^3A'$ and $^3A''$ complexes. That the energy between the $^3A'$ and $^3A''$ complexes is greater in the MPn than HF calculations may result from the different effects treating electron correlation has on the geometries of these two complexes. For the $^3A''$ complex the MP2 O···H distance is 0.06 Å shorter than is the HF O···H distance. The difference between the MP2 and HF O···H distances is larger, i.e., 0.13 Å, for the $^3A'$ complex. Thus, if shortening of the O···H distance by MP2 theory leads to an increased stability of the complex, MP2 geometry optimization will stabilize the $^3A'$ complex more than the $^3A''$ complex.

(25) *CRC Handbook of Chemistry and Physics*, 65th ed.; Weast, R. C., Ed.; CRC Press: Boca Raton, FL, 1984.

TABLE IV: Geometry and Energy of the Planar $^3A'$ Complex

coordinate[a]	HF[b]	MP2[b]	ref 14 (HF)
R_1	0.957	0.978	0.957
R_2	2.075	1.943	2.003
R_3	0.954	0.984	0.953
R_4	1.306	1.317	1.305
α	91.9	80.5	104.3
β	144.0	140.6	147.5
γ	105.1	103.5	104.5

theory	total electronic energy[c]	electronic binding energy, kcal/mol
HF	-225.574 53	6.00
	-225.627 2 (ref 14)	4.6
MP2	-226.062 83	9.55
MP3	-226.074 56	8.55
MP4	-226.095 97	9.28
PHF	-225.577 03	4.16
PMP2	-226.058 55	8.94
PMP3	-226.076 18	8.25
PMP4	-226.097 60	8.99
CI (SD)	-226.084 2 (ref 14)	6.3
CI(SDQ)	-226.132 5 (ref 14)	5.3

[a] Bond lengths and angles are in units of angstroms and degrees, respectively. The coordinates are defined in footnote *a* of Table I. [b] The 6-31G** basis set was used for the HF and MP2 calculations. [c] Energies are given in hartrees. The HF energy is calculated at the HF geometry. The remaining energies (except those from ref 14; see text) are calculated at the MP2 geometry. The MP2 energy is full; the PHF, MP3, MP4 and all PMPn energies are frozen core.

In previous work Toohey and Anderson[15] also calculated the geometry and energy of the $^3A'$ complex using HF/6-31G** theory. Our results in Table IV for this level of theory are identical to what they reported. Jackels and Phillips[14] performed the first ab initio study of the $^3A'$ complex. The geometry they found is listed in Table IV. It was determined using HF theory and the standard 6-31G** basis set, except that the polarization functions were chosen to have exponents of 0.85 on oxygen and 1.0 on hydrogen instead of the standard values of 0.8 and 1.1, respectively. These different polarization function exponents explain why their HF optimized $^3A'$ hydrogen-bonded complex has a slightly different geometry than does ours. Using a polarized double-ζ basis set, HF, CI(SD) and CI(SDQ) energies were then calculated for this optimized geometry.[14] These energies are listed in Table IV, where they are compared with the results of our study. We would expect the CI(SD) and CI(SDQ) methods to give a more strongly bound $^3A'$ complex if the complex's geometry had been optimized at these higher levels of theory instead of using the HF optimized geometry.

D. Nonplanar Potential Energy Surfaces. As discussed above, on the $^3A'$ surface the planar HO···HO_2 hydrogen-bonded species has a lower energy than on the $^3A''$ surface. However, as one moves along the reaction path in the direction of products, the $^3A''$ surface eventually becomes lower in energy since it correlates with the ground electronic state products while the $^3A'$ surface correlates with excited electronic state products. This crossing can occur either before or after the $^3A''$ transition state is reached, as illustrated in Figure 4.

In nonplanar configurations an avoided crossing occurs between the $^3A'$ and $^3A''$ surfaces. As illustrated in Figure 5, the nature of the resulting nonplanar potential energy surface is strongly affected by the position of the $^3A'$–$^3A''$ avoided crossing. If the crossing occurs before the $^3A''$ transition state, the nonplanar transition state for the lowest energy ^3A surface arises from the

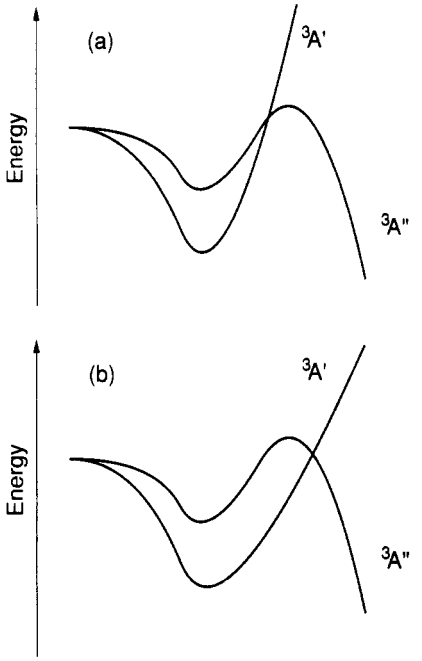

Figure 4. Two possible $^3A'$–$^3A''$ surface crossings.

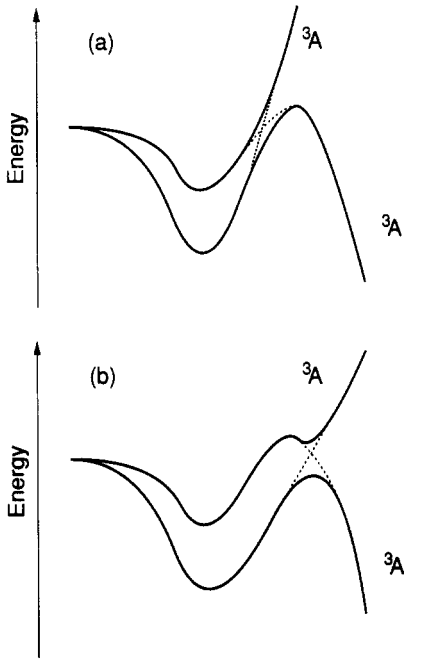

Figure 5. Nonplanar avoided crossings for the $^3A'$–$^3A''$ surface crossings in Figure 4.

planar transition state for the $^3A''$ surface. However, if the avoided crossing occurs after the planar $^3A''$ transition state is reached, the remnants of the planar $^3A''$ transition state are now on the *upper* ^3A surface, and the transition state for the *lower* ^3A surface arises from the avoided crossing between the $^3A'$ and $^3A''$ surfaces.

The position of the $^3A'$–$^3A''$ crossing was determined for different levels of theory, by calculating a $^3A'$ energy at the $^3A''$ transition-state geometry. If the $^3A'$ energy is higher, the crossing occurs before the $^3A''$ transition state is reached. At the HF/6-31G** optimized $^3A''$ transition-state structure and for energies calculated at this level of theory, the $^3A'$ surface is 2.1 kcal/mol *higher* than the $^3A''$ surface. Thus, at this level of theory the nonplanar ^3A surfaces are like those in Figure 5a. For the MP2/6-31G** optimized $^3A''$ transition-state structure, both HF/6-31G** and MP2/6-31G** energies were determined. The resulting $^3A'$ energy is 3.7 kcal/mol *lower* and 1.3 kcal/mol *higher* than the $^3A''$ energy for the HF and MP2 energies, respectively. Therefore, the nonplanar ^3A potential energy surfaces are like those in parts b and a of Figure 5 for the HF and MP2 energies, respectively.

TABLE V: Comparison of the Planar $^3A''$ Transition State and the Nonplanar ^3A Transition State Originating from the Planar $^3A''$ Transition State

coordinate[a]	planar	nonplanar[e]
	Geometries[b]	
θ_1	0.0 (0.0)	4.8 (4.8)
θ_2	0.0 (0.0)	81.0 (81.0)
R_1	0.973 (0.953)	0.972 (0.953)
R_2	1.332 (1.240)	1.339 (1.238)
R_3	1.064 (1.114)	1.059 (1.113)
R_4	1.259 (1.259)	1.297 (1.260)
α	99.1 (101.7)	105.8 (103.5)
β	160.2 (167.6)	160.0 (165.8)
γ	107.7 (109.9)	106.9 (108.6)
	Frequencies[c]	
	2130i (5185*i*)	2211i (5239*i*)
	3824 (4086)	3860 (4087)
	2449 (1636)	3635 (1379)
	2297 (1380)	1452 (1363)
	1761 (867)	1274 (1310)
	1464 (647)	710 (737)
	705 (636)	396 (466)
	423 (189)	297 (221)
	256i (99*i*)	102 (100)
	Energies[d]	
HF	−225.533 14	−225.533 44
MP2	−226.043 64	−226.043 00
MP3	−226.051 77	−226.051 54
MP4	−226.077 61	−226.077 00
PHF	−225.547 23	−225.548 12
PMP2	−226.041 38	−226.040 38
PMP3	−226.054 77	−226.054 34
PMP4	−226.080 61	−226.079 80

[a] $\theta_1 = H_1$–O_2–H_3–O_4 dihedral and $\theta_2 = O_2$–H_3–O_4–O_5 dihedral. The remaining coordinates are defined in footnote *a* of Table I. Bond distances are in units of angstroms and angles in degrees. [b] Both MP2/6-31G** and HF/6-31G** optimized geometries are given. The HF geometries are in parentheses. [c] See footnote *a* of Table II. [d] See footnote *c* of Table I. [e] Severe SCF convergence difficulties (probably due to the proximity of the two states as shown in Figure 5) as well as the flatness of the potential energy surface with respect to the dihedral angles θ_1 and θ_2 prevented the usual convergence on the optimized geometry. With θ_1 and θ_2 fixed at their HF optimized values, the maximum gradient (0.000 40 au) and RMS gradient (0.000 15 au) of the MP2 optimized structure were below the usual thresholds. From further attempts at optimization, we estimate the uncertainty in θ_1, θ_2, and the MP2 energy to be ±10°, ±40°, and ±0.001 au, respectively.

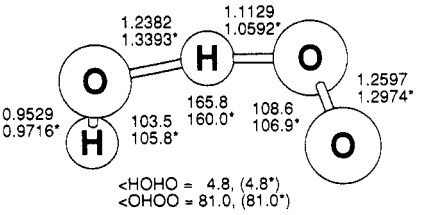

Figure 6. Calculated HF and MP2 (indicated by asterisks) geometries for the nonplanar ^3A transition state, which originates from the planar $^3A''$ transition state.

E. Nonplanar $^3A''$ Transition State. The planar constraint used to determine the HF and MP2 $^3A''$ second-order transition state given in Table II and Figure 2 was relaxed to determine the true nonplanar ^3A transition state originating from this second-order transition state. Optimized structures of this nonplanar transition state were obtained at both the HF and MP2 levels of theory and are listed in Table V and depicted in Figure 6. Also listed in Table V are energies and vibrational frequencies for the nonplanar transition state.

Relaxing the planar constraint allows the planar ^3A transition state to take nonzero dihedral angles. However, as shown in Table V, the remaining internal coordinates are nearly identical for the

planar $^3A''$ and nonplanar ^3A transition states. The difference between the HF and MP2 geometries for the nonplanar transition state is the same as discussed above for the planar transition state. The MP2 calculation gives a much earlier transition state than does the HF calculation. A major difference between the planar and nonplanar transition states, at both the HF and MP2 levels of theory, lies in their vibrational frequencies. The planar $^3A''$ and nonplanar ^3A transition states have very similar energies, with the nonplanar one *lower* by 0.19 kcal/mol for the HF calculations. The potential energy surface is very flat with respect to rotation out of the plane, changing by only 0.5 kcal/mol at both the HF and MP2 levels as θ_2 is changed from 0 to 90°.

This nonplanar ^3A transition state will be the OH + $HO_2 \rightarrow$ H_2O + $^3O_2$ reaction transition state if the $^3A'$ and $^3A''$ surfaces cross as shown in Figure 4a to give the nonplanar ^3A surfaces shown in Figure 5a. As discussed in section II.D, calculations with HF/6-31G** geometries and energies and MP2/6-31G** geometries and energies show that the $^3A'$–$^3A''$ crossing is that given in Figure 4a. However, we do not feel the calculations reported here are sufficiently quantitative to rule out the possibility that the actual $^3A'$–$^3A''$ crossing occurs after the $^3A''$ transition state. Second-order Møller–Plesset perturbation theory probably does not adequately treat the coupling between the $^3A'$ and $^3A''$ surfaces in nonplanar configurations, and a multi-reference CI calculation[27] may be necessary for a proper representation of this coupling. If the crossing occurs after the $^3A''$ transition state, the nonplanar ^3A transition state found here will not be the reaction transition state.

III. Reaction Kinetics

A. Ab Initio Rates. The ab initio calculations reported here give a transition state for reaction on the triplet surface with a potential energy greater than that of the reactants. Thus, these calculations predict a *positive* activation energy for reaction in contrast to the *negative* activation energy observed in experimental measurements[1,3] of the reaction rate.

The nonplanar MP2 transition-state structure, MP2 vibrational frequencies, and PMP4 transition-state energy (Table V), when combined with the MP2 reactant properties (Tables I and II), give a transition-state theory rate constant for reaction 1 at 300 K of 1.2×10^{-15} cm^3 molecule^{-1} s^{-1}, with Arrhenius parameters of $A = 4.7 \times 10^{-13}$ cm^3 molecule^{-1} s^{-1} and $E_a = 3.58$ kcal/mol. These rate parameters differ sharply with those found in the most recent experimental determination[1] of k_1 for the 254–382 K temperature range; i.e., $k_1 = (4.8 \pm 0.8) \times 10^{-11} \exp[(250 \pm 50)/RT]$ cm^3 molecule^{-1} s^{-1}. The ab initio rate constant is too small by 4 orders of magnitude, which results from an ab initio A factor and activation energy that are too small and too large, respectively. Thus, the ab initio transition state is tighter and has a higher potential energy than the one that controls the experimental reaction rate.

The above analysis indicates that the kinetics for the experimental reactive system is not controlled by a transition state along the reaction path which has properties like those of the ab initio transition state found here. One way to ensure that crossing this transition state is not rate controlling is to simply lower its potential energy. If the MP2 transition-state structure and vibrational frequencies are assumed as above, the transition state's electronic potential energy relative to reactants must be lowered by 7.5 kcal/mol to −5.8 kcal/mol to obtain a rate constant which agrees with the experimental value of 9.2×10^{-11} cm^3 molecule^{-1} s^{-1} determined by Keyser[1] at the highest temperature he investigated of 382 K. At lower temperatures this modified transition state gives rate constants larger than the experimental values so that crossing this modified ab initio transition state is not rate controlling for all temperatures in the range investigated by Keyser.

B. Vibrational/Rotational Adiabatic Capture Rate Constant. If the tight ab initio transition state discussed above does not control the rate of reaction 1, the rate must be controlled by the long-range interaction between OH and HO_2.[15] A model for this interaction is the dipole–dipole intermolecular potential,[28] which is given by

$$(-\mu_1\mu_2/R^3)[2\cos\theta_1\cos\theta_2 - \sin\theta_1\sin\theta_2\cos(\phi_1 - \phi_2)] \quad (4)$$

In this equation μ_i is the absolute magnitude of the dipole moment and (θ_i, ϕ_i) refer to the spherical polar angles describing the orientation of r_i, with respect to the body-fixed axes, for molecule i. This equation provides a basis for calculating a capture rate constant[29] for OH + HO_2 association. Capture supposedly occurs when the reactive system moves inside a critical value for the center of mass separation R between the two molecules. After capture, it is assumed the reactive system forms the $^3O_2$ + H_2O products with unit efficiency.

There are different theoretical approaches for calculating the capture rate constant. One could use either microcanonical or canonical variational transition-state theory (VTST), with the canonical version giving an upper bound to the more accurate microcanonical rate constant.[29] A Langevin type classical mechanical theory[17,29] can also be used to calculate the capture rate constant. Here we use vibrationally/rotationally adiabatic theory[30–32] to calculate the capture rate constant. In this theory it is assumed that quantum numbers for reactant energy levels can be used to label adiabatic potential energy curves versus reactant separation and that the reactive system stays on the same energy curve with fixed quantum numbers until the critical reactant capture radius is attained.[32] A properly evaluated vibrationally/rotationally adiabatic rate constant will be less than or equal to that of microcanonical VTST.[31]

For the dipole–dipole potential in eq 4 the vibrationally/rotationally adiabatic capture rate constant is found to be[32]

$$k(T) = p_e(T)1.766(\pi/\mu)^{1/2}(\mu_1\mu_2)^{2/3}(k_BT)^{-1/6} \quad (5)$$

where $p(T)$ is the probability the collision occurs on the reaction potential energy surface,[33,34] μ is the reactant reduced mass, and k_B is the Boltzmann constant. The term $p(T)$ is the electronic partition function ratio and, for OH + HO_2, is given by

$$p(T) = \frac{g^\ddagger}{Q_{e,OH}Q_{e,HO_2}} \quad (6)$$

For OH + HO_2 association, reaction occurs on a ^3A potential energy surface so that $g^\ddagger = 3$. The ground state of HO_2 has $^2A''$ symmetry and the $^2A'$ first excited state is approximately 17 kcal/mol higher in energy,[35] so that for thermal energies Q_{e,HO_2} is 2. The OH radical has $^2\Pi_{3/2}$ and $^2\Pi_{1/2}$ low-lying spin–orbit states, with the $^2\Pi_{1/2}$ state $205R$ higher in energy.[33] Thus

$$Q_{e,OH} = 2 + 2\exp(-205/T) \quad (7)$$

$$p(T) = \frac{3}{2[2 + 2\exp(-205/T)]} \quad (8)$$

Theoretical values for k_1 are determined by inserting eq 8 into eq 5 and using the HO_2 and OH dipole moments of 2.09 and 1.67 D,[14] respectively. The resulting k_1 rate constants versus temperature are given by the chain-dashed line in Figure 7.

C. Comparison between Theoretical and Experimental k_1 Rate Constants. There have been two experimental measurements of the temperature dependence of k_1 which can be compared with the above theoretical analysis. In early work by Sridharan et al.,[3]

(26) Howard, C. J. *J. Am. Chem. Soc.* **1980**, *102*, 6937.
(27) Bernardi, F.; De, S.; Olivucci, M.; Robb, M. A. *J. Am. Chem. Soc.* **1990**, *112*, 1737.
(28) Hirschfelder, J. O.; Curtiss, C. F.; Bird, R. B. *Molecular Theory of Gases and Liquids*; Wiley: New York, 1954; p 27.
(29) Hase, W. L.; Wardlaw, D. M. In *Bimolecular Collisions*; Ashfold, M. N. R., Baggott, J. E., Eds.; Royal Society of Chemistry: London, 1989; p 171.
(30) Marcus, R. A. *J. Phys. Chem.* **1979**, *83*, 204.
(31) Quack, M.; Troe, J. *Ber. Bunsen-Ges. Phys. Chem.* **1974**, *78*, 240.
(32) Clary, D. C. *Mol. Phys.* **1984**, *53*, 3.
(33) Clary, D. C.; Werner, H.-J. *Chem. Phys. Lett.* **1984**, *112*, 346.
(34) Graff, M. M.; Wagner, A. F. *J. Chem. Phys.* **1990**, *92*, 2423.
(35) Gole, J. L.; Hayes, E. F. *J. Chem. Phys.* **1972**, *57*, 360.

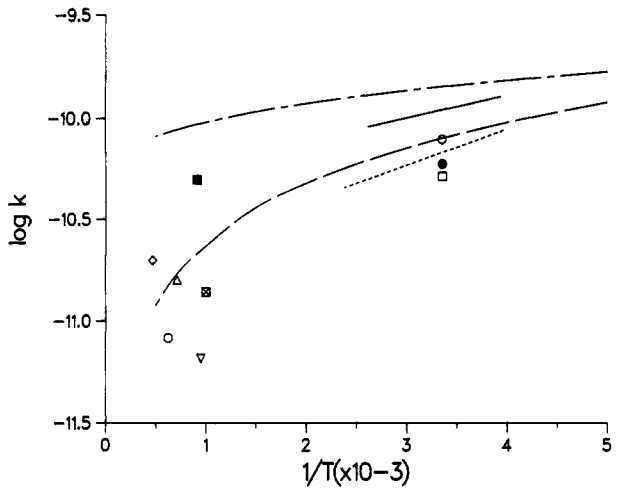

Figure 7. Rate constants for OH + HO_2 reaction: (---) theoretical, this work; (—) expt;[1] (---) expt;[3] (○) expt;[2] (□) expt;[36] (●) expt;[37] (■) expt;[38] (△) expt;[39] (◇) expt;[40] (▽) expt;[41] (○) expt;[42] (□) expt;[43] (---) compilation.[44]

k_1 was found to equal $(1.7 \pm 0.5) \times 10^{-11} \exp[(416 \pm 86)/T]$ cm^3 molecule^{-1} s^{-1} for T = 252–420 K. More recently,[1] Keyser found that $k_1 = (4.8 \pm 0.8) \times 10^{-11} \exp[(250 \pm 50)/T]$ cm^3 molecule^{-1} s^{-1} for T = 254–382 K. Rate constants determined from these expressions are plotted versus temperature in Figure 7, for the temperature ranges considered in the experiments. The agreement between the experimental rate constants by Keyser[1] and those determined here is quite good for the 250–400 K temperature range. The maximum discrepancy is 50% at 400 K. The theoretical values for k_1 in Figure 7 give $k_1 = 9.32 \times 10^{-11} \exp(124/T)$ cm^3 molecule^{-1} s^{-1} for T = 250–400 K. The expression $k_1 = 1.17 \times 10^{-10}(T/300)^{-0.21} \exp(113/RT)$ fits the theoretical k_1 for the T = 200–2000 K temperature range.

Schwab et al.,[2] Rozenshtein et al.,[36] and Dransfeld and Wagner[37] have measured k_1 at 298 K, and these values are included in Figure 7. Values for k_1 measured at high temperatures ($T \geq 1000$ K)[38-43] are also shown in Figure 7. The rate constant reported by Hippler et al.[38] for T = 1100 K is only a factor of 2 smaller than that predicted by our theoretical model. From an assessment of all the experimental data prior to 1986, Tsang and Hampson[44] suggested that k_1 have the temperature dependence $k_1 = 2.4 \times 10^{-8} T^{-1}$ cm^3 molecule^{-1} s^{-1}. Rate constants from this expression approach our theoretical values at low temperatures but are too small at high temperatures.

D. Effect of the Theoretical k_1 on Combustion Simulation. Reaction 1 plays an important role as a chain-terminating step following

$$H + O_2 + M = HO_2 + M \qquad (9)$$

in the combustion of fuel-lean mixtures as has been demonstrated by a comparison of computer-simulated OH profiles to those measured experimentally in propane–air flames.[45] The OH density immediately beyond the flame zone in the fuel-lean flame (ϕ = 0.63) described in this reference is far above thermal equilibrium and decreases in the burned gas toward equilibrium over a distance of several millimeters. The shape of the OH decay profile is controlled in large part by the formation and subsequent consumption reactions of HO_2 in this region of the flame.

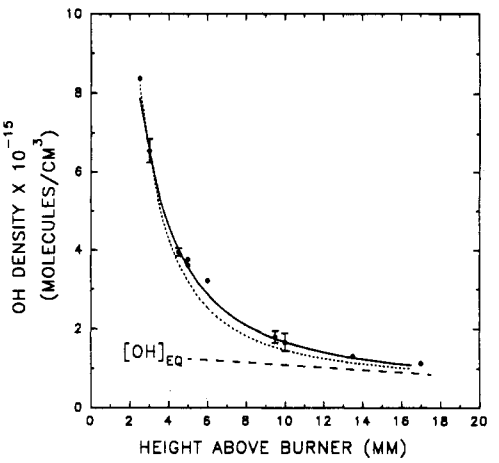

Figure 8. OH profiles in propane–air flames: (···) and (—) are computer simulations, see text; (●) expt.[45]

The calculated temperature dependence of k_1 determined here (see Figure 7) can be combined with the average rate constant for all experimental measurements at 298 K ($=8.6 \times 10^{-11}$ cm^3 molecule^{-1} s^{-1}) to obtain a "best" estimate of the absolute value and temperature variation of k_1:

$$k_1 = 7.1 \times 10^{-11}(T/300)^{-0.21} \exp(113/RT)$$

Evaluating this rate expression at 1100 K gives a value of 5.7×10^{-11} cm^3 molecule^{-1} s^{-1} in excellent agreement with the recent measurement of Hippler et al.[38] (i.e., 5.0×10^{-11}) but significantly larger than earlier high-temperature measurements of k_1 (see Figure 7). We believe that this new rate expression is that preferred for modeling high-temperature combustion systems. At 1700 K, this value of k_1 is a factor of 7 larger than that used in the simulations of ref 45. The effect of this new value of k_1 on the simulated OH profile is shown in Figure 8. Individual points in this figure represent experimental data,[45] and the dotted curve is obtained using the above value of k_1 with the other rate constants from Table I of ref 45. Evidently, changing the value of k_1 produces a significantly steeper OH decay profile and a poorer fit to the data.

Since the publication of ref 45, a new measurement of the temperature dependence of k_9 has become available[46] in both N_2 and H_2O diluents. The value of this rate constant in the burned gas mixture at 1700 K is approximately 35% smaller than that used previously,[45] primarily because of a reduction in the measured collision efficiency of H_2O relative to N_2 at higher temperature. Therefore, we have carried out a new fit to the OH decay curve in the lean flame using the rate constants of ref 45 with the exception that k(OH + HO_2) was changed to expression k_1 above and $k(H + O_2 + N_2) = 6.5 \times 10^{-33} \exp(1350/RT)$ was used.[46] The collision efficiency for H_2O at 1700 K was determined to be 3.66,[46] and that of CO_2 was estimated to be 2.0. All other efficiencies were set equal to that of N_2 (=1.0). No data are available for the CO_2 collision efficiency, but it is likely that it is somewhat larger than N_2 and smaller than H_2O. A value of 1.0 for CO_2 would, in fact produce an imperceptible change in the quality of the fit. The solid line in Figure 8 is the fit obtained using these new rate constants and collision efficiencies. The agreement with the experimental data is excellent.

IV. Discussion

A. Triplet Electronic Structure Calculations. One of the most interesting aspects of the OH + HO_2 reaction is the relationship between the planar potential energy surfaces for the $^3A''$ and $^3A'$ electronic states and the two nonplanar ^3A potential surfaces, which originate from these planar surfaces. The ground-state products H_2O and $^3O_2$ correlate with the $^3A''$ state. However,

(36) Rozenshtein, V. B.; Gershenzon, Yu. M.; Il'in, S. D.; Kishkovitch, O. P. *Chem. Phys. Lett.* **1984**, *112*, 473.
(37) Dransfeld, P.; Wagner, H. G. *Z. Naturforsch* **1987**, *42a*, 471.
(38) Hippler, H.; Troe, J.; Willner, J. *J. Chem. Phys.* **1990**, *93*, 1755.
(39) Troe, J. *Ber. Bunsen-Ges. Phys. Chem.* **1974**, *72*, 946.
(40) Friswell, N. J.; Sutton, M. M. *Chem. Phys. Lett.* **1972**, *15*, 108.
(41) Day, M. J.; Thompson, K.; Dixon-Lewis, G. *14th Symp. (Int.) Combust.* **1973**, 47.
(42) Peeters, J.; Mahnen, G. *14th Symp. (Int.) Combust.* **1973**, 133.
(43) Dixon-Lewis, G.; Rhodes, P. *Dewxieme Symp. Eur. Combust.* **1975**, 473.
(44) Tsang, W.; Hampson, R. F. *J. Phys. Chem. Ref. Data* **1986**, *15*, 1087.
(45) Kaiser, E. W. *J. Phys. Chem.* **1988**, *92*, 4384.
(46) Hsu, K.-J.; Anderson, S. M.; Durant, J. L.; Kaufman, F. *J. Phys. Chem.* **1989**, *93*, 1018.

since the $^3A'$ hydrogen-bonded complex HO···HO_2 has a potential energy ~4 kcal/mol lower than that for the $^3A''$ complex (see Tables III and IV), the ground-state nonplanar potential energy surface initially followed by the reactants correlates with the $^3A'$ surface. At shorter reactant separations the $^3A''$ and $^3A'$ surfaces cross, which becomes an avoided crossing in nonplanar configurations. As shown in Figures 4 and 5 there are two different general locations for this crossing.

In the calculations presented here the structure of the nonplanar ^3A transition state, which correlates with the $^3A''$ transition state, is determined. Though calculations of energies and optimized structures at the HG/6-31G** level and the MP2/6-31G** level indicate that the $^3A''$–$^3A'$ crossing is that depicted in Figures 4a and 5a, it is not felt that the calculations reported here are sufficiently accurate to rule out the possibility that the crossing in Figures 4b and 5b is correct. For example, calculations with MP2/6-31G** optimized geometries and HF/6-31G** energies give the crossing in Figures 4b and 5b. We feel that multireference CI calculations[27] may be needed to establish the definitive nature of the $^3A''$–$^3A'$ crossing.

The size and temperature dependence of the experimental rate constant for reaction 1 indicate that the reaction rate is controlled by the long-range OH + HO_2 attractive potential.[2] The nonplanar ^3A transition state found here is much "too tight" to be consistent with the experimental A factor. Thus, for passage of this transition state to not be rate controlling, the transition state's potential energy must be substantially less than that of the reactants. However, the nonplanar ^3A transition state found in this work has a PMP4 potential energy 1.5 kcal/mol higher than that of the reactants. If this is the proper transition state for the ground-state ^3A surface, its potential energy must be lowered by 3.3 kcal/mol to be consistent with the experimental rate constant. However, as discussed above, this ^3A transition state is the reaction transition state only if the $^3A''$–$^3A'$ crossing occurs before the $^3A''$ transition state (Figure 4). If the actual crossing occurs after the $^3A''$ transition state, the true ^3A reaction transition state will differ from the ^3A transition state found here and should have a lower potential energy, in better agreement with the experimental requirement.

B. Reaction Mechanism. The calculations reported previously for the singlet potential energy surface[18] and those reported here for the triplet potential energy surface provide considerable insight into the OH + HO_2 reaction mechanism. On the singlet surface OH and HO_2 associate to form the excited trioxide molecule H_2O_3*. Since a high potential energy barrier is calculated for H_2O_3* decomposition to H_2O + $^1O_2$, this decomposition becomes important only at highly elevated temperatures.[18] This result agrees with an earlier isotopic study of Kurylo et al.[8] They studied the reaction between ^{18}OH and $H^{16}O_2$ and observed only a very small signal from $^{18}O^{16}O$. Thus, at thermal temperatures H_2O_3* decomposes to reactants and there is no reaction on the singlet surface. Loss of OH from OH + HO_2 collisions on the singlet surface will occur if the H_2O_3* is collisionally stabilized. However, this is predicted to require pressures in excess of 5000 Torr for the commonly used bath gas He.[18]

From the work presented here, it is concluded that on the triplet surface OH and HO_2 react without a potential energy barrier to form H_2O and $^3O_2$. Reaction rate constants calculated for the triplet surface and based on the reactants long-range dipole–dipole potential, agree with OH loss experimental rate constants for the 250–1100 K temperature range. The indication from this comparison is that except at extremely high pressures where H_2O_3* becomes collisionally stabilized, the loss of OH occurs on the triplet surface. Since the rates for the OH + HO_2 → H_2O_3* reaction on the singlet surface and the OH + HO_2 → H_2O + $^3O_2$ reaction on the triplet surface are both controlled by the reactants long-range dipole–dipole potential, the ratio of H_2O_3* to H_2O + $^3O_2$ formation is predicted to be given by the electronic state degeneracies and is $^1/_3$. Therefore, if the bath gas pressure is increased to stabilize H_2O_3*, the rate constant for the loss of OH would increase by 33%.

The above theoretical model can be compared with the experimental study of Dransfeld and Wagner.[37] They studied the ^{18}OH + $H^{16}O_2$ reactive system at room temperature and low pressures and found equal rates (within statistical uncertainties) for

$$^{18}OH + H^{16}O_2 \rightarrow H_2{}^{18}O + {}^{16}O_2 \quad (10a)$$

$$^{18}OH + H^{16}O_2 \rightarrow {}^{16}OH + H^{18}O^{16}O \quad (10b)$$

The ab initio calculations reported here and in ref 18 indicate reaction 10a occurs on the triplet surface and reaction 10b occurs on the singlet surface by trioxide formation and ensuing decomposition, with one-half of the trioxide decomposing by reaction 10b. Therefore, the result of Dransfeld and Wagner[37] indicates that the rate of OH + HO_2 association on the singlet surface to form H_2O_3* is twice the rate of OH + HO_2 → H_2O + $^3O_2$ on the triplet surface. This differs significantly from our prediction that the rate of H_2O + $^3O_2$ formation to H_2O_3* formation is 3/1.

An explanation of the above difference is not obvious. As discussed before,[37] impurities in the experimental reaction system may have affected the experimental findings. It is also possible that the electronic adiabatic model we have assumed for the singlet and triplet surfaces should be modified. In this model it is assumed that the singlet and triplet reactions only occur on the ground-state ^1A and ^3A surfaces, respectively. It is possible that spin-allowed electronic transitions between the ground and excited ^1A states and the ground and excited ^3A states should be included. In addition, dynamical effects (see the following) may be important.

Because of a basic assumption in our theoretical model, the theoretical rate constant for the triplet surface may be too large at high temperatures. The theoretical model for the rate constant is based on the reactant long-range dipole–dipole potential in eq 4. This potential does not differentiate between the two reactant orientations HO···HO_2 and HO_2···HO. The former leads directly to products without an overall potential energy barrier, while the latter encounters a repulsive potential barrier at short reactant separations. However, the theoretical expression for $k_1(T)$, eq 5, is based on the assumption that both orientations form products.[32] As the temperature is increased there is less time for an unfavorable orientation to reorient as the reactants interact. However, this effect might be compensated by the increased reactant angular velocities at high temperatures. Nevertheless, eq 5 may overestimate $k_1(T)$ by up to a factor of 2 at high temperatures. It would be interesting to study reaction 1 by classical trajectory calculations.[47]

Acknowledgment. This research was supported by the Ford Motor Company Scientific Research Laboratories and the Institute for Manufacturing Research at Wayne State University. These calculations were performed in part at the NSF Pittsburgh Supercomputing Center. The authors thank Ling Zhu for assisting in the rate constant calculations.

Registry No. HO_2, 3170-83-0; OH, 3352-57-6.

(47) Vande Linde, S. R.; Hase, W. L. *J. Chem. Phys.* **1990**, *93*, 7962.